Characterisation of Clustered Cracks using an ACFM Sensor and Application of an Artificial Neural Network

Rowshandel, Hamed; Nicholson, Gemma; Shen, J. l.; Davis, Claire

DOI:
10.1016/j.ndteint.2018.04.007

Accepted Manuscript

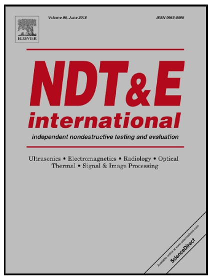

Characterisation of Clustered Cracks using an ACFM Sensor and Application of an Artificial Neural Network

H. Rowshandel, G.L. Nicholson, J.L. Shen, C.L. Davis

PII: S0963-8695(17)30381-X

DOI: 10.1016/j.ndteint.2018.04.007

Reference: JNDT 1975

To appear in: *NDT and E International*

Received Date: 21 June 2017

Revised Date: 25 March 2018

Accepted Date: 12 April 2018

Please cite this article as: H. Rowshandel, G.L. Nicholson, J.L. Shen, C.L. Davis, Characterisation of Clustered Cracks using an ACFM Sensor and Application of an Artificial Neural Network, *NDT and E International* (2018), doi: 10.1016/j.ndteint.2018.04.007

Characterisation of Clustered Cracks using an ACFM Sensor and Application of an Artificial Neural Network

H. Rowshandel[1], G.L. Nicholson[1], J.L. Shen[2], C.L. Davis[1,2]

1 Birmingham Centre for Railway Research and Education, University of Birmingham, Birmingham B15 2TT, UK
2 Advanced Steel Research Centre, WMG, University of Warwick, Coventry, CV4 7AL, UK

Abstract. The alternating current field measurement (ACFM) technique can be applied for surface-breaking fatigue crack detection and sizing; the link between the ACFM signal and crack size is well understood for individual cracks. However, the ACFM response to multiple clustered cracks is significantly different to that of isolated cracks. In railway rails the high wheel-rail forces can lead to rolling contact fatigue (RCF) cracks. Often cracks appear together in small clusters or in long stretches. The accurate characterisation of such fatigue cracks is essential for carrying out efficient and safe repair and maintenance. This paper presents a method for sizing the important sub-surface section of multiple cracks using ACFM via the application of an artificial neural network (ANN). The approach is demonstrated using a railway case study: a simulation-based dataset of signal response covering the range of RCF cracks typically seen in in-service railway tracks has been generated to give a thorough representation of the effect of clustered crack parameters on the ACFM response. A 5×5×2×1 multi-layer ANN has been optimised and trained using the validated simulation database to learn the inverse relationship between the crack pocket length (desired output) and the ACFM signal for a given cluster of RCF cracks. The network has been evaluated on a set of experimental data to size cracks of known dimensions from ACFM measurements and also on unseen simulation data. Results from both simulation and experiment show that the approach presented can be used to size clustered cracks to approximately the same degree of accuracy as is possible for isolated cracks.

Keywords: ACFM, automated fault diagnosis, clustered cracks, ANN

1. Introduction

Fatigue cracks are a common cause of concern in most industries where metals are in service. Electromagnetic (EM) testing techniques are often used to detect and characterise cracks in safety-critical components in, for example, the oil and gas, nuclear, aeronautical and railway industries. Defect characterisation uses a model of the interaction between EM sensors and defects (see, for example, [1, 2]). It requires a solution to the inverse problem to be found, that is, for an unknown defect to identify the sub-surface size of the defect corresponding to a measured signal.

Some analytical solutions for specific circumstances exist, e.g. the forward problem for eddy current testing [3] and a solution to the inverse problem for planar semi-elliptical cracks is possible for ACFM [4] due to the locally uniform electromagnetic field. Numerical solution techniques for the inverse problem are more common and applicable to more diverse crack shapes and conditions [5-12]. Huge computational power may, however, be required to solve complex inversion problems numerically. Artificial intelligence based methods have been used to reduce the inversion problem to a simpler classification task [13-15].

In the railway industry, rolling contact fatigue (RCF) cracks in rails occur due to the high contact stresses between the wheel and rail, present even during normal operating conditions. It can be difficult to interpret the information received during inspection, that is, to determine the relationship between the signals received from inspection hardware and the size of the defects under test. This task is nearly always complicated by the presence of clusters of multiple closely-spaced cracks compared to isolated cracks [16, 17]. Following the fatal and economically damaging Hatfield, UK, rail derailment [18] inspection of the British railway network revealed more than 2000 sites of potentially serious RCF cracks [19]. At the derailment site over 300 cracks were discovered, and the rail had fragmented into over 200 pieces. As at this site, RCF cracks in rails often appear in clusters, with the cracks typically between 2 and 20 mm apart [20]. Characterisation of clustered cracks using EM testing approaches has only rarely been reported [21].

The alternating current field measurement (ACFM) technique can be used for RCF crack detection in rails. Network Rail, the GB infrastructure manager, has investigated the use of an ACFM sensor contained in a walking stick system [22, 23]. Models have been developed to relate the ACFM signal to crack size (via the pocket length) for isolated RCF cracks [24] whilst more recent work has shown the ACFM response for real RCF cracks within clusters is very different to that of isolated cracks and that there is a non-linear relationship between the signal response and the geometry of the cracks in the cluster [20, 24, 25].

Due to the increased number of parameters that can affect the ACFM signal for crack clusters (crack size, spacing, and number in a cluster) compared to isolated cracks, calibration curves as used for sizing isolated cracks are not sufficient when considering the sizing of crack clusters. In this paper a machine learning approach using an artificial neural network (ANN) is applied to the problem of sizing RCF cracks within clusters using ACFM measurements. To achieve this, extensive modelling work, based on defect parameters observed in railway clustered RCF cracks, has been undertaken to determine the influence of important crack parameters on the ACFM signal, and to be used as the training and validation databases for the ANN. D'Angelo, et al. [61] proposed a method for automatic classification of isolated defects from 2D scans using Lissajous figures. While this method can be only applied on isolated cracks, it has potential to be further extended to allow extraction of this method’s a priori information about crack clusters from 2D scans.

2. NDT techniques in the railway industry

Railway inspection via NDT has been practised for almost 100 years since the introduction of a mobile magnetic flux leakage based system for defect detection by Sperry [26]. More recently, conventional ultrasonic (UT) sensors have been the dominant technique for inspection of deep cracks in rails. It requires liquid coupling between sensor and the rail and more importantly, suffers from what is known as "crack shadowing", where the presence of smaller crack(s) within a cluster of cracks may block the identification of larger and more critical ones [27].

A number of other NDT techniques have been investigated and introduced for the detection of RCF cracks in the railway industry. Pulsed EMATs (electromagnetic acoustic transducers) can be used without contact, although they are sensitive to lift-off effects and exhibit low sensitivity to small defects [28]. Amongst electromagnetic NDT techniques, magnetic flux leakage (MFL), eddy current (EC), and ACFM have been shown to be the most applicable techniques for the detection and characterisation of small surface-breaking defects in metals. MFL can be used in surface-breaking and shallow subsurface crack detection for cracks >4mm long, although MFL sensors suffer from rapid performance deterioration at speed [26, 29, 30]. EC and ACFM can reliably detect small to medium surface-breaking cracks, and the latter has the added benefit of higher sensitivity to surface cracks and lower sensitivity to sensor lift-off than the former [31-33]. Automated NDT for fault diagnosis and condition monitoring is becoming increasingly common due to the advancement in sensor technology combined with the computational efficiency of modern electronics [34-37]. For a comprehensive overview of the NDT techniques used in the railway industry, the reader is referred to [26].

No individual NDT technique has been able to fully meet all of the requirements of railway rail condition inspection, namely, robust and reliable detection, deployment at speed and accurate defect characterisation capability for small and larger cracks. Combined systems have been deployed on rail measurement trains, for example the Deutsche Bahn system [38] using EC and UT technologies. When operating at high speed, inspection is typically limited to detection or categorisation of severity such as reported by [39] in a system combining UT, EC and visual technologies; the authors suggest employing a machine learning approach for improved defect classification using the signals received from their system.

The combination of artificial intelligence (AI) methods with NDT in the railway industry has been proposed or reported a number of times [40, 41]. For example, in the automatic processing of image based techniques: for track profile inspection [42], detection of missing track-to-sleeper fastening bolts [43], and defect detection in sleepers and fastenings [44]. Automatic classification of defective wooden sleepers and quantification of surface length and width of cracks was reported in [45] using multi-layer perceptron and support vector machines. Automatic detection of defects in freight car wheels [46] and axles [47] via AI techniques to process the signals from UT testing has also been reported.

Accurate characterisation, over and above purely detection, of the cracks formed within clusters remains to be achieved by the majority of the NDT techniques applicable for RCF crack inspection on the railway. Some results in this area have been reported using pulsed eddy current thermography. Such an approach, combined with infrared (IR) imaging, has been applied to the visualisation of multiple cracks in a rail in a laboratory environment [21]. It shows the potential to quantify the subsurface geometry of cracks within clusters, including the angle and depth. Transfer to an operational railway environment may be hindered by the potential fragility of the imaging equipment in a harsh environment and restrictions on deployment of the technique at speed. A static PEC thermography approach is used and an initial investigation conducted into determining defect depths and orientations by extracting the thermal response at the crack tip over time [48]. Hesse et al., [17] investigated the use of a surface wave inspection technique and considered clusters of cracks. It was found that the interference between signals did not allow precise sizing, but it was suggested that some categorisation of severity may be possible.

3. Overview of the ACFM Principle

The ACFM technique induces a locally unidirectional alternating current (AC) into a specimen under inspection. This current flows in a thin skin near the surface; the presence of a crack will force the current to flow around the ends and down its faces. These changes in the direction of the current will produce non-uniformity in the magnetic field which is constantly monitored by an ACFM instrument. The ACFM instrument is moved across or just above the surface of a specimen under test and sensors measure two of the components of the magnetic field, that is, tangent to the specimen surface (B_x) and perpendicular to the direction of induced current flow (B_z). As the current passes down and around the face of a crack a reduction in current intensity produces a trough in the B_x signal over the centre of the crack. The maximum reduction from the background level in the B_x signal, $\Delta B_{x_{max}}$, (see Figure 1) can be related through inversion of the ACFM signal to the crack's pocket length, i.e., the length of the crack along its direction of propagation below the surface.

When clusters of closely-spaced cracks are inspected with an ACFM instrument the B_x signal does not return to its background level between cracks. For very closely spaced cracks (<5mm, approximately, depending on size), distinct troughs are not observed in the one dimensional B_x signal, and for more widely spaced cracks indistinct individual troughs may be present [33]. The maximum change in B_x from a scan over the whole cluster is greater than for an individual crack of the same size, as shown in the example in Figure 1. While solutions to the inverse problem for isolated cracks are well established, using analytical [23, 49], numerical [24, 50] or empirical [23] methods, the determination of the subsurface size of cracks appearing in clusters is not yet fully reported, and is the subject of the remainder of this paper via a combined modelling and ANN approach. It will also be shown that sizing of clustered RCF cracks based on the technique that is already established for single RCF cracks could result in a large margin of error.

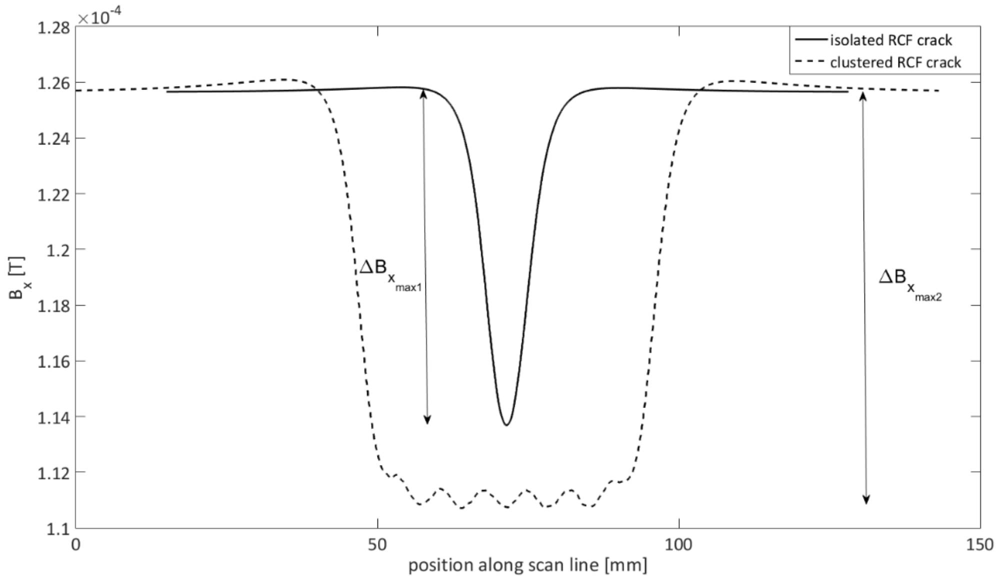

Figure 1 Comparison of the ACFM signal between an isolated and clustered crack. The results correspond to a crack of 10 mm surface length and aspect ratio of 1.5 where the clustered crack consists of 7 uniform cracks of the same size as the isolated crack having an inter-crack spacing of 5 mm.

4. Modelling Approach

The non-linear nature of the equations governing the interaction of the ACFM signal with a defect makes it impractical to obtain a general closed-form solution and invert the ACFM signal. An analytical solution to the inverse problem for isolated cracks of semi-elliptical geometry exists [49], but within the ACFM walking stick product tested on the GB railway calibration and empirical destructive testing were used to generate look up tables for crack sizing since the analytical model gave inaccurate results [23]. Another common approach is the application of the finite element method (FEM) to solve the distribution of the magnetic field in the air above the defect and tabulation of the measured ACFM signal and respective crack size using the modelled data [32]. In this study, a uniform field COMSOL model previously developed for isolated RCF cracks [20, 24, 50, 51] has been extended to allow a wider parametric study of clustered RCF cracks closely enough spaced that their ACFM signals overlap (see Figure 2). In the model the material properties of the air and the metal domains are: conductivity (σ) 50 and $5x10^6$ S/m, respectively, and relative magnetic permeability (μ_r) 1 and 50, respectively. A non-zero value of air conductivity is used to avoid singularity issues when solving the forward problem with the FEM solver. In the simulation step, the probe has been modelled using a uniform field approximation, validated in previous work [20, 24, 50, 51] to simplify resolving the FEA model for each probe position and to speed up the computations. Therefore, in the model a uniform incident field has been applied to the conductor domain and the solution of the disturbed magnetic field intensity (i.e. B_x and B_z) above the cracks in the air domain has been sampled at different positions along the centre line of the crack cluster at a fixed spacing of 0.142 mm.

4.1 Modelled Crack Parameters

The focus of this study is on the application of ACFM in the railway industry. Hence, the range of parameters used for the cracks in the model was chosen to represent RCF cracks at their early stage of development where the cracks have not yet turned down into the rail and can be removed by grinding. The crack parameters of interest for this study are crack surface length (S), inter-crack spacing (I), i.e., the average perpendicular distance between the centre of the surface components of the cracks, number of cracks in a cluster (N). Crack aspect ratio (R) describes the ratio of the major axis (a) to the minor axis (b) of an ellipse; the value of the major axis is given, assuming the minor axis is 1, thus a ratio of 1.5:1 is denoted R = 1.5. The crack vertical angle (V) was fixed at 30° [20, 24] while a crack width of 0.5 mm is used in this model. Shen, et al. [52] showed that, for RCF cracks propagating into a rail at a range of angles from 30-90°, the ACFM B_x signal response to changing crack vertical angle is insignificant. Hence, the B_x signal can be directly used to determine the crack pocket length.

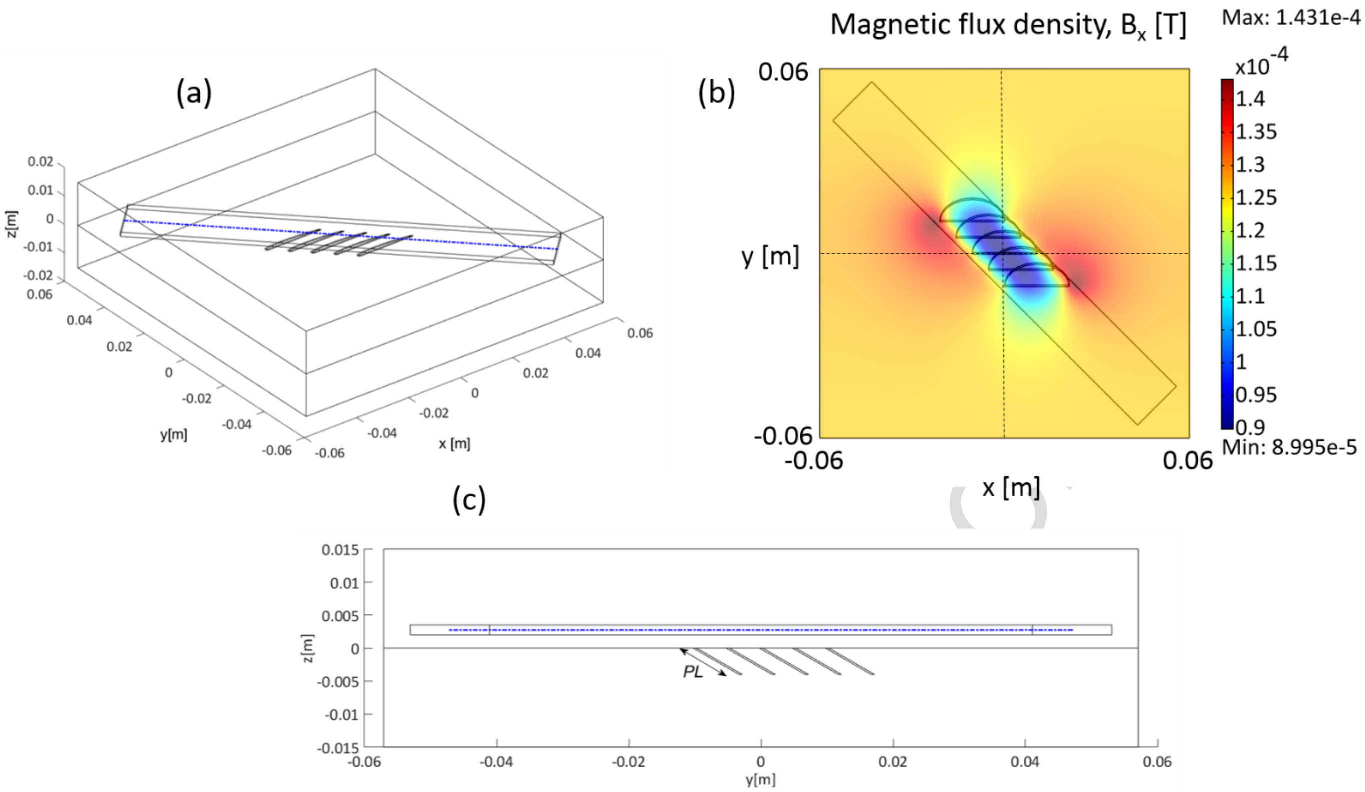

Figure 2 An example of the 3D COMSOL model used for study of the ACFM response to clustered RCF cracks in rails; in this case S = 20 mm, R = 1.25, I = 5 mm and V = 30°. The dotted blue line is the position where the solution of magnetic flux density is extracted to simulate a 1D scan along the rail in the isometric (a) and side (c) views; view (b) shows the top view of the B_x field solution.

The range of values of the parameters S,R, I and V were chosen based on observations of samples taken from in-service rails in earlier studies [53-55]. The parameter N was limited to 15 as the maximum deviation observed in the ACFM signal saturates for N > 15. The ACFM magnetic field measurements were extracted at a constant, pre-calibrated distance from the surface, corresponding to a zero lift-off measurement by the commercial ACFM sensor that has been used to validate the simulation results. The cracks are assumed to be planar and semi-elliptical, which matches well with empirical observations of small and moderately sized RCF cracks, while it is an appropriate simplification in the case of some heavier cracks which have not turned down into the rail [24]. However, errors in sizing will arise for the larger cracks as deviations from semi-elliptical shapes occur (discussed in [25]) therefore this approach is most suited to sizing small and moderate cracks with the aim to determine required grinding depth for maintenance procedures. Cracks within clusters of RCF observed in rail are often of similar size to one another, although this is not always the case. Uneven sizes may be observed, for example, when there is mixed traffic using a line; in a case like this crack shadowing is a potential problem for UT inspection. Therefore, some of the RCF clusters used in this study were modelled with the middle crack in the cluster being larger than the neighbouring cracks in terms of both the surface length and pocket length in order to study the robustness of the ANN in sizing such clusters. The parameter M specifies the ratio of the pocket length of the middle crack in a cluster to that of its neighbouring cracks. Table 1 gives a summary of the values used for the parameters of interest.

Table 1 Values of the clustered crack parameters used in the model.

Parameter	Note	Unit	Value
S	Crack surface length	mm	1,2,4,5,6,7,8,9,10,12,14,15,16,18,20,22,24,25,26,28,30
I	inter-crack spacing	mm	1,2,4,6,8,10,12
N	Number of cracks in a cluster	-	3,5,7,9,11,13,15,17
R	Crack aspect ratio	-	1,1.25,1.5,1.75
V	Crack vertical angle	°	30
M	Ratio of the largest surface length to the smallest surface length	-	1,1.25,1.5,1.75,2,2.25,2.5,2.75,3,3.2,3.5,3.7

In this study, a total of 1985 different sets of clustered cracks were simulated to represent a range of RCF crack clusters. The simulation time depends on the scale and complexity of each model as well as the processing power of the host platform; for the range of parameters considered in this study, a single simulation's run time varied between approximately 60 and 500 s on a 64-bit operating system with quad core Intel processor running at 3.2 GHz and memory of 16 Gb. Figure 2(b) shows the x-component of the magnetic field, B_x, in two dimensions for an example crack cluster. The one-dimensional B_x signal extracted along the centre line of the solution domain is normalised with respect to the background signal, B_{x_0}, taken at a location away from the cracks where the induced current is undisturbed. This provides the means to compare the modelling results with experimental measurements obtained from an ACFM instrument with digitised output. In each case, the normalised maximum signal reduction, i.e., $\frac{\Delta B_{x_{max}}}{B_{x_0}} \times 100$, is obtained from the FEM solution. Determining the relationship between this value and the pocket length given the number of cracks, the inter-crack spacing and their surface length is the target of this study.

4.2 Analysis of the modelling results

The effect of the parameters I and N on $\frac{\Delta B_{x_{max}}}{B_{x_0}} \times 100$ was studied to help understand the non-linear ACFM response to clustered cracks (see Figure 3 and Figure 4). The normalised magnetic field scan lines ($\frac{B_x}{B_{x0}} \times 100$) for a sample of the cases is shown in Figure 5 and Figure 6 which correspond to the data shown in Figure 3 and Figure 4.

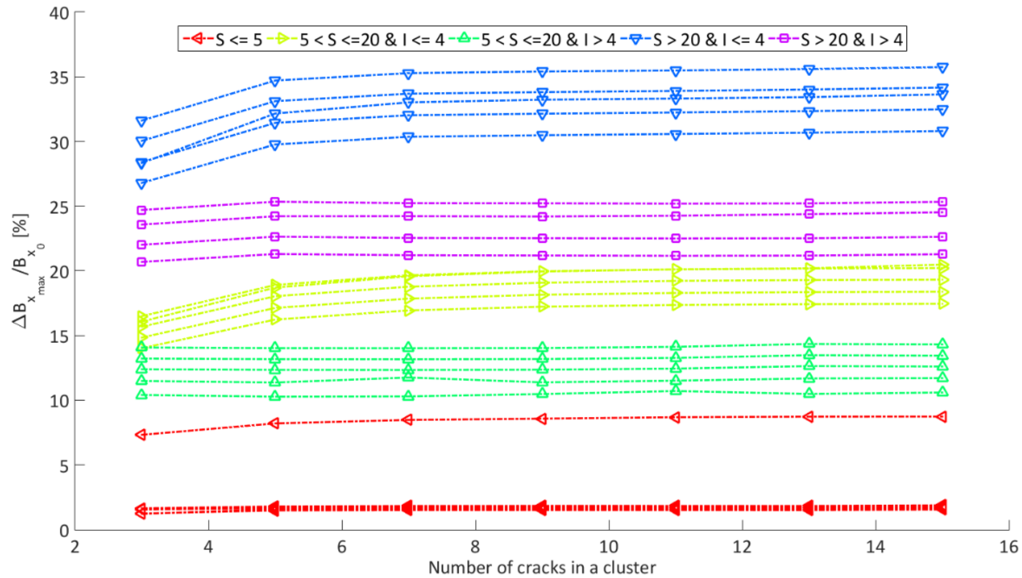

Figure 3 Effect of number of cracks in a cluster (N) on the ACFM signal. Each curve represents a different set of constant parameters values of S, R and I.

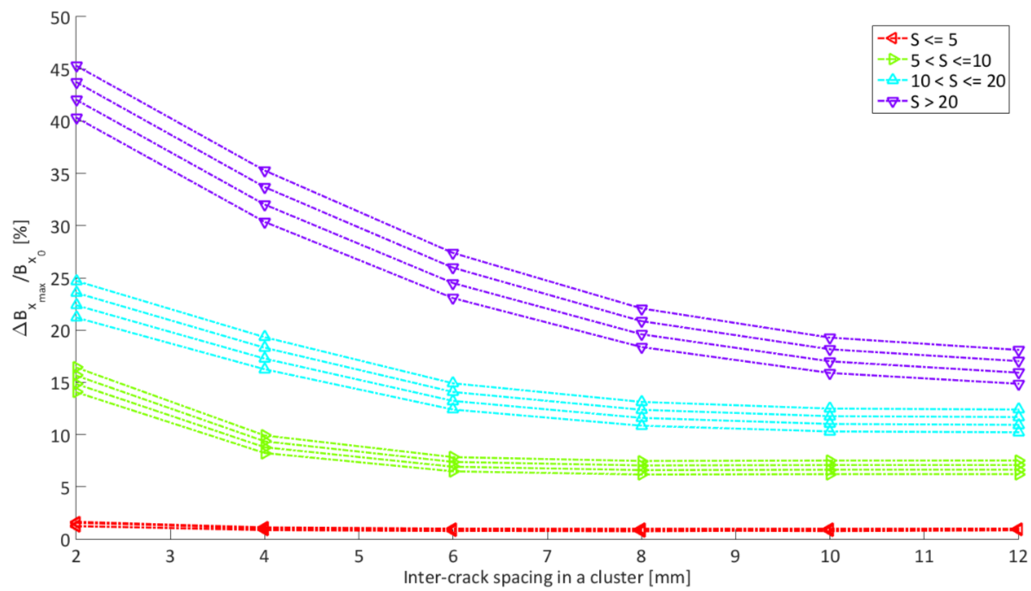

Figure 4 Effect of inter-crack spacing (I) on the ACFM signal. Each curve represents different sets of constant parameters (S, R and N).

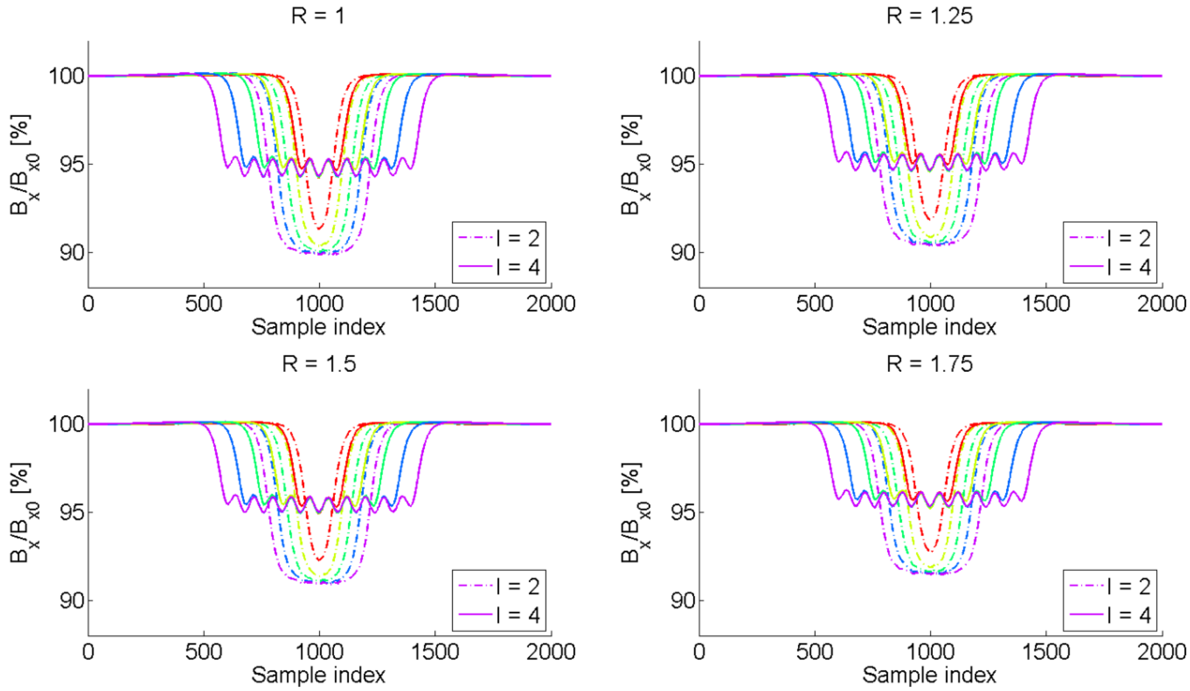

Figure 5 Effect of N (odd numbers from 3 to 11) on the ACFM signal for cracks of small surface length for different values of I and R (here S = 5 mm). Curves represent the magnitude of the x-component of the magnetic field B_x along the centre line of the solution box. In the case of I = 4 mm the individual cracks in a cluster can be distinguished.

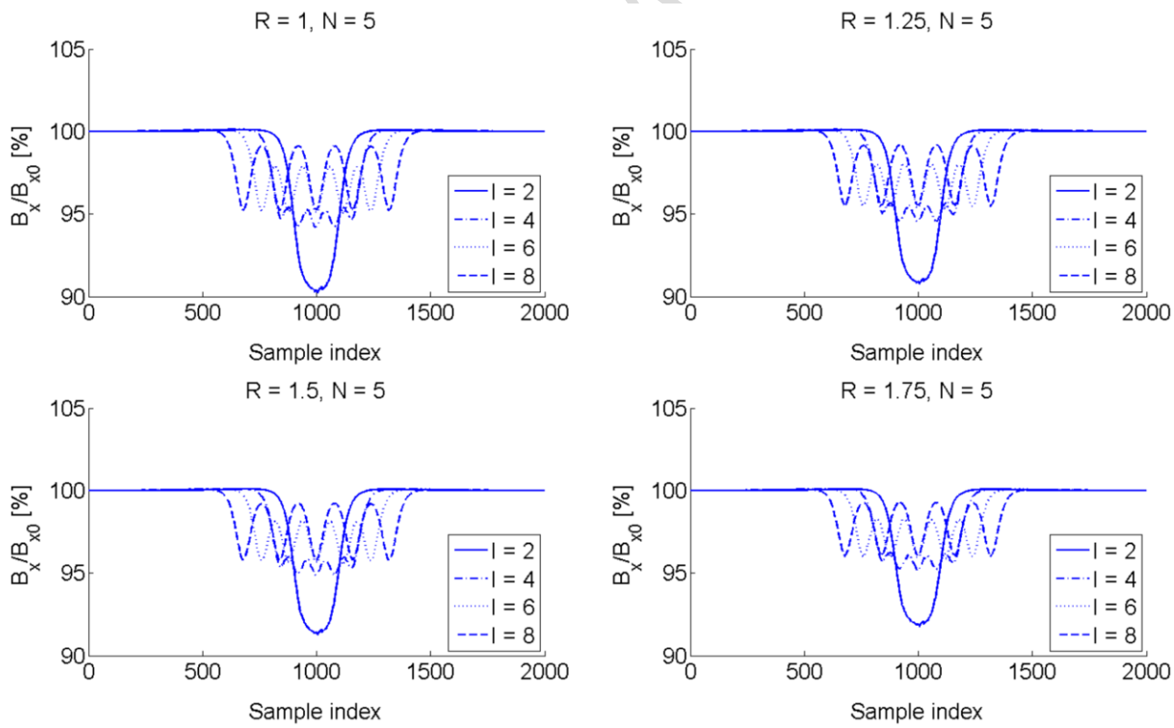

Figure 6 Effect of I on the ACFM signal for cracks of small surface length for different values of N and R (here S = 5 mm). Curves represent distribution of the x-component of the magnetic field B_x along the centre line of the solution box.

Figure 3 shows complex behaviour where the effect of N on the ACFM signal is dependent on the values of S and I. For $S \leq 5$ mm the influence of the number of neighbouring cracks on the maximum reduction in the magnetic field is insignificant, which suggests that individual cracks in a closely-spaced cluster behave as an isolated crack, whereas for $S > 5$ mm the effect of N on the signal depends only on the value of I. This dependency weakens with increasing I and nearly vanishes for $I > 4$ mm while it intensifies with decreasing I. Further, the overall dependency on N vanishes for $N > 11$. Less complex behaviour, however, is observed in Figure 4 where the effect of I on the signal is mostly dependent on the value of S; this dependency intensifies with increasing S and weakens with decreasing S until it nearly vanishes for $S < 5$ mm. The overall dependency on I vanishes for $I > 10$ mm in the case of S < 20 while there is still a weak dependency for S > 20.

4.3 Comparison with single crack sizing method

In order to demonstrate the significance of these dependencies on crack sizing using established techniques, a calibration curve currently used for sizing of isolated RCF cracks using ACFM measurements [24] was referred to in order to evaluate its accuracy for sizing of clustered cracks. To achieve this, eight of the modelled crack clusters were selected, Table 2. These clusters were also machined into a steel calibration plate (Figure 7) and experimental ACFM measurements were taken. For ease of machining vertical cracks were produced in the calibration plate, noting that for V >30° there is no effect of vertical angle on the B_x value [48].

Table 2 Parameters of RCF clusters used for extra validations.

Cluster	C1	C2	C3	C4	C5	C6	C7	C8
S, mm	5	7	11	15	21	14	5	10
PL, mm	2	2	4.4	5	6	7	2	4
R	1.25	1.75	1.25	1.5	1.75	1	1.25	1.25
I, mm	3	3	5	4	7	5	8	8
N	3	7	3	5	7	7	7	7
Comments	-	-	-	-	-	-	middle crack is bigger S = 15, PL = 5	middle crack is bigger S = 15, PL = 5

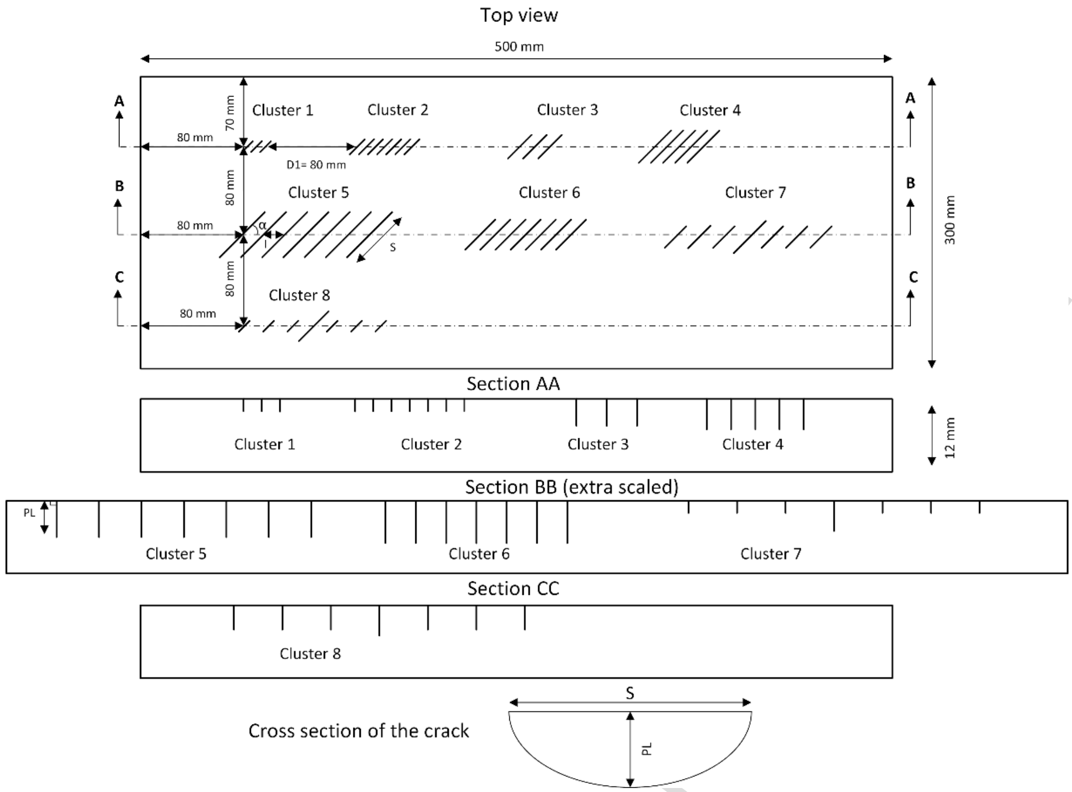

Figure 7 Illustration of the calibration block used for experimental validation.

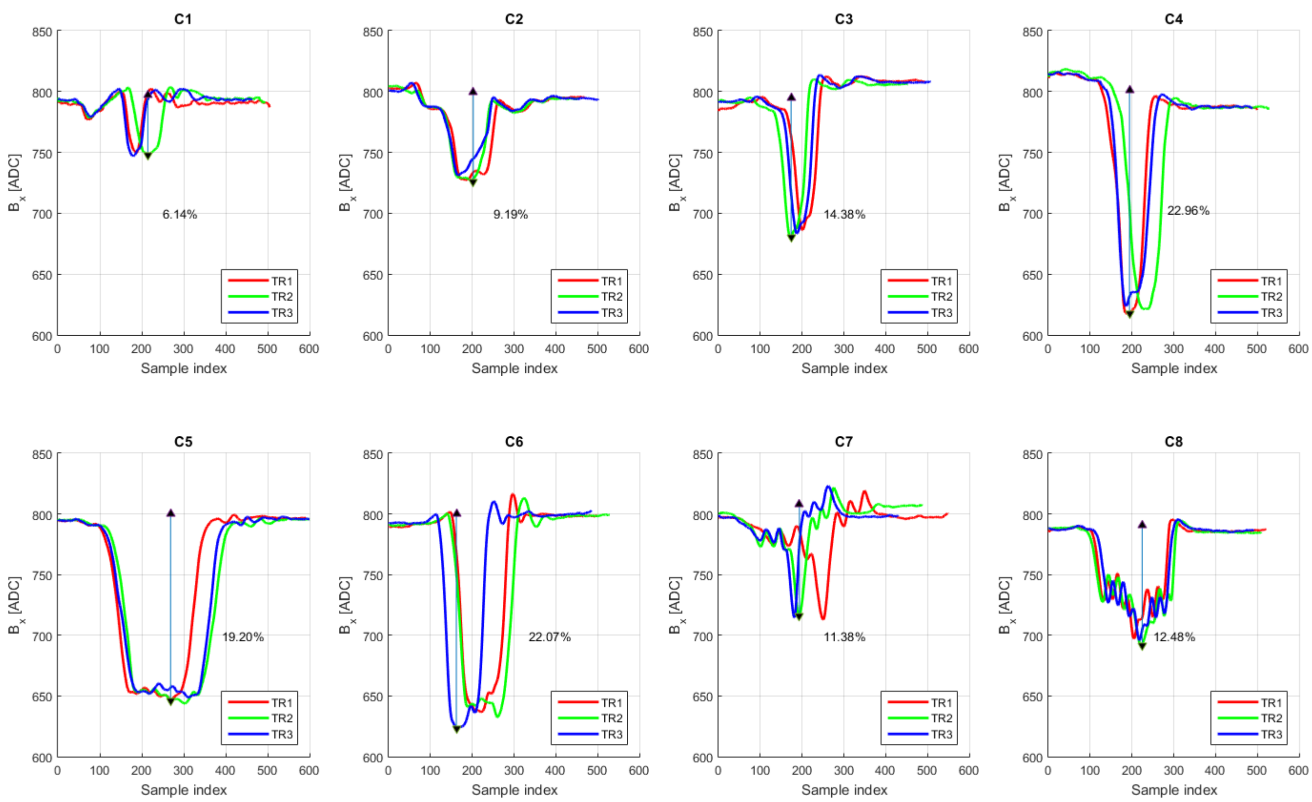

Figure 8 Experimental ACFM B_x field measurements using a single probe sensor over the cracks in the calibration block. TR1 denotes trial number 1 while C1 denotes cluster 1, etc.

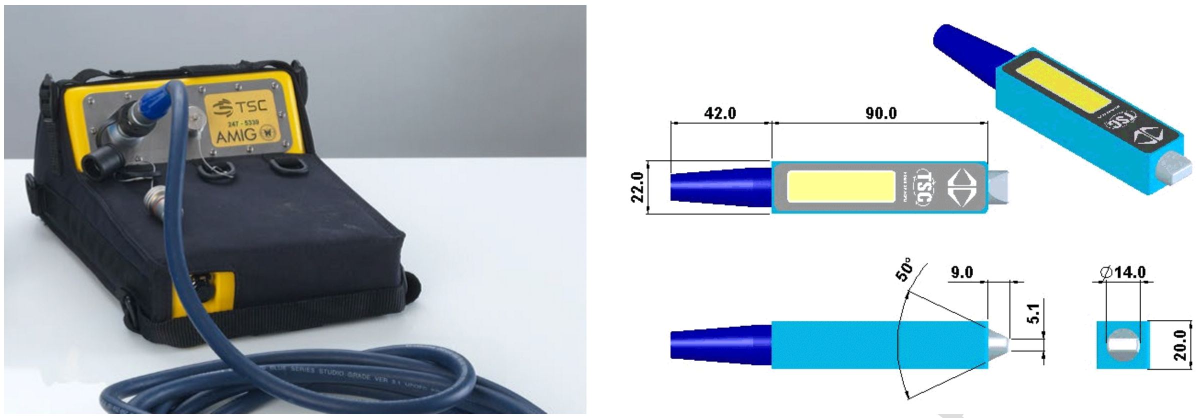

(a) (b)

Figure 9 (a) Image of the ACFM instrument and (b) illustrations of the ACFM probe used for the experimental measurements (linear dimensions are in mm) [56].

Figure 8 shows the experimental B_x measurements obtained along the scan line passing through the centre of the cracks of the calibration sample (dashed line in Figure 7) using a commercial ACFM instrument as shown in Figure 9. The design of the probe is based on a cylindrical coil carrying 5 kHz AC current to induce a current in a specimen and two orthogonal "micro" cylindrical coils for measuring the flux density in two directions namely B_x and B_z. Based on the manufacturer's specifications, the instrument uses a 16 bits resolution ADC system and the instrument has a repeatability of 5 ADC units and an output date rate of 100 Hz. (The high speed sampled data are buffered internally by the instrument for signal conditioning purposes before the instrument streams the data to the PC). The probe can be used to size cracks of 1 mm deep so, as long as the changes in the overlapping signals due to closely spaced cracks compares to the level of a signal for a 1 mm deep crack (approximately 1% normalised value for a crack with surface length of 2.5 mm based on the calibration curve), then the instrument should be able to resolve it. In the experimental work, the probe was moved over the cracks by hand at low speed. Each measurement was repeated three times and the signal from the trial which resulted in the maximum signal reduction was taken. The corresponding signal reduction was converted to a normalised value (i.e. $\frac{\Delta B_{x_{max}}}{B_{x_0}} \times 100$). For the eight clusters this value has been plotted against the surface length of the cracks in Figure 10, alongside the single crack sizing calibration curves.

In the sizing method for isolated cracks, given the maximum normalised ACFM signal drop (i.e. $\frac{\Delta B_{x_{max}}}{B_{x_0}} \times 100$) over the crack and the crack surface length, the crack pocket length may be estimated, assuming a certain semi-elliptical shape. The calibration curves in Figure 10 represent the B_x signal drop of semi-elliptical cracks whose shape is representative of the extremes expected in RCF cracks, that is between semi-circular (R = 1) and whose width is 3.5 times their pocket length (R = 1.75), refer to Figure 10. As such, the measured ACFM B_x signal drop should fall between the upper and lower lines for a known surface length. The pocket length is inferred from the ellipse ratio of the line on which the measurement falls or interpolated when the measurement is between lines.

As can be observed in Figure 10, the signal drop for clusters C1 – C6 falls above all of the curves when plotted against the actual surface length. Using the sizing method for isolated cracks this would suggest elliptical ratios of R < 1 in each case, when the true elliptical ratios are R = 1 (C6), R = 1.25 (C1, C3), R = 1.5 (C4) and R = 1.75 (C2, C5). In fact, the measurements suggest elliptical ratios much less than 1; by interpolation C6 gives approximately R = 0.5, indicating a pocket length of 21 mm since the surface length is 21 mm. The true pocket length is 6 mm, which is severely overestimated by this method. Since the other values are proportionally even further from the R = 1 curve for the remaining clusters, C1 – C4 and C6, interpolating a ratio value is inadvisable and would lead to gross overestimations of pocket length.

The situation is slightly different for clusters C7 and C8 which each contain 6 smaller cracks and one central larger crack with longer surface length and pocket length. For these clusters the measured B_x signal drop has been plotted against the surface length of the largest crack per cluster, which is 15 mm in both cases. For C8 interpolating using this surface length value gives an elliptical ratio of R = 1.95 and therefore a pocket length of 3.85 mm, which undersizes the largest crack (which has 5 mm pocket length), but is close to the pocket length of the remaining cracks (4 mm). If the average surface length (10.7 mm) were to be used as input to the method, the pocket length would be found to be 5.35 mm. In the case of C8, using the surface length of the largest crack gives a correct estimation of the pocket length of the largest crack, which is 5 mm via an elliptical ratio of R = 1.5. If the average surface length, 6.4 mm, were to be used the interpolation method would be infeasible since the marker falls far from the upper curve. Even for this limited sample of two unevenly sized clusters it can be seen that the sizing method is unreliable, and only by chance was an accurate measure obtained for C8.

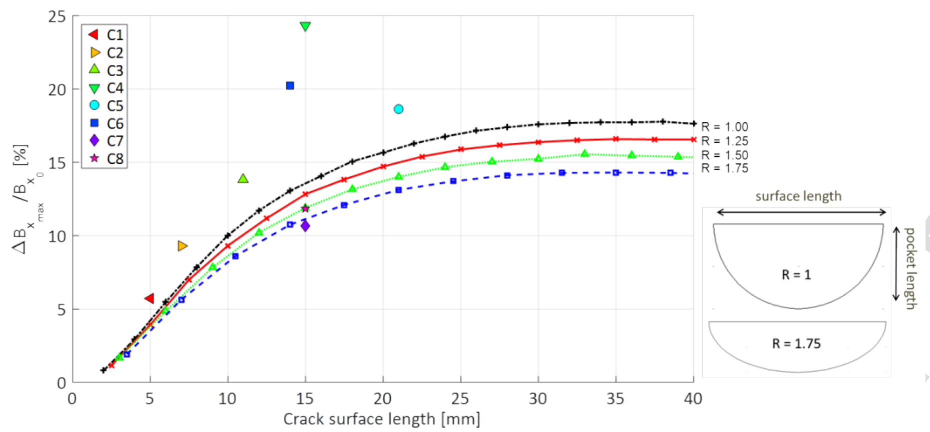

Figure 10 Experimental ACFM measurements of clusters C1 – C8 plotted against the calibration curve used for sizing isolated cracks. In the case of uneven clusters (C7 & C8), the maximum surface length corresponding to the middle crack was used.

To address the problem of sizing cracks in a cluster a machine learning approach is proposed where the crack pocket length is predicted by an ANN which is trained to learn the inverse relationship between the ACFM signal and crack pocket length based on a training database obtained via modelling. An earlier study by Ravan, et al. [57, 58] proposed a neural network approach to reconstruct isolated cracks of multi-humped profile from ACFM measurements, although this network would not generalise to the characterisation of clustered cracks. In the present study, the inversion aims to map inputs from domain R^{+5} to R^{+} through a non-linear network to predict the crack pocket length (PL), given S, I, N, M and $\frac{\Delta B_{x_{max}}}{B_{x_0}}$. In this paper, the parameters S, I, N and M are given by prior knowledge of the RCF cracks. Methods exist to detect these automatically. For example, S and M can straightforwardly be obtained from the B_z signal [32] while I and N can be obtained using a camera and image processing techniques [59, 60]. D'Angelo, et al. [61] proposed a method for automatic classification of isolated defects from 2D scans using Lissajous figures. While this method can be only applied on isolated cracks, it has potential to be further extended to allow extraction of this method's a priori information about crack clusters from 2D scans.

5. Architecture of the ANN

This section describes the ANN architecture designed for the specific problem of clustered crack sizing. Different architectures of the network design were initially considered including networks with both a single hidden layer and multiple hidden layers, however, a multilayer perceptron (MLP) neural network was finally used, consisting of one input layer, two hidden layers and one output layer (Figure 11) as it showed a better generalisation capability. A tansigmoid function has been used as the activation function for the hidden layer due to its non-linear and saturation properties for inputs of large absolute values. This is very appealing in the context of the ACFM response to clustered cracks where the signal has been shown to saturate with respect to parameters I and N, as seen in Figure 3 and Figure 4. A linear transfer function has been used for the output layer. The Bayesian regularization (BR) method was used for training the network using backpropagation.

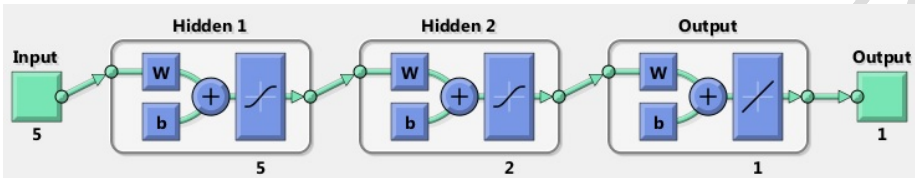

Figure 11 Architecture of the ANN network use as a non-linear regression estimator. Numbers denote the number of neurons used in each layer while w and b represent weights and biases used in each layer

5.1 Training Method

To train the network, 70% of the simulated RCF crack models were used, including uneven clusters where $M \neq 1$. The training set was selected such that it includes cracks covering the whole range of surface lengths modelled. This is a crucial step in training a network that aims to allow the network to generalise well, since the ACFM response to the parameters of interest has been shown to be different for the different crack categories. Furthermore, the network was trained ten times using different random weights and biases and the network with the best performance was used for further analysis. The average training time was approximately 15 s. This reduces the effect of weight initialisations and poor convergence due to being trapped in a local minimum during training and contributes to a more reliable network with better accuracy and reliability than a network which is trained once. The result of training is shown in Figure 12. All the data sets, i.e., training, validation and test sets were assessed to analyse the prediction accuracy and generalisation of the network. It can be seen that all the different categories of RCF cracks were included in each dataset. The results show that the network can predict the pocket length of a uniform RCF crack cluster with a good accuracy, i.e., to within ± 10%.

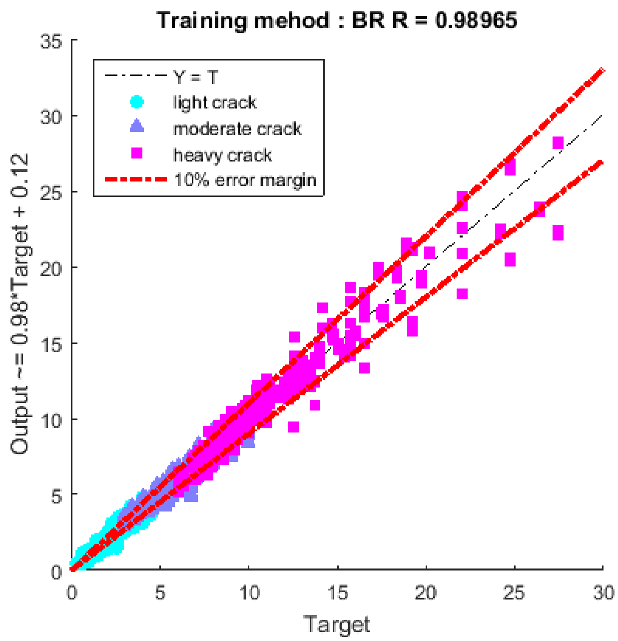

Figure 12 Evaluation of the trained network over the whole dataset.

5.2 Sensitivity Analysis

In order to analyse the accuracy of the trained network in crack sizing from experimental measurements, which usually contain some measurement error, the network inputs were subjected to random white noise of varying signal-to-noise ratio (a time-based seed was used for generation of random numbers to effectively model independence of input parameters). The effects of the noise in some input parameters on the network output, crack pocket length, were studied. In doing so, the first, second and fourth parameters were considered for the analysis as the parameter *N* is visually measured. In each case, one parameter was subject to an additive white noise error while the other two parameters were kept constant. The results (see Figure 13) suggest that the network is most sensitive to the fourth parameter, $\frac{\Delta B_{x_{max}}}{B_{x_0}}$, and least sensitive to the first and second parameters (i.e. *S* and *I*).

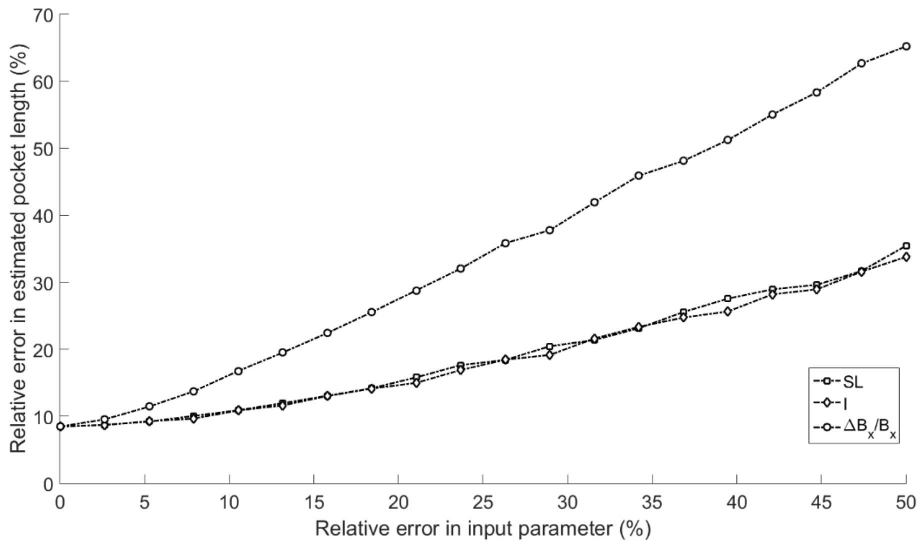

Figure 13 Plot of the network sensitivity to the input parameters S, I and $\frac{\Delta B_{x_{max}}}{B_{x_0}}$. Results are averaged over training, validation and test sets.

6. Results and Discussion of the Network Validation

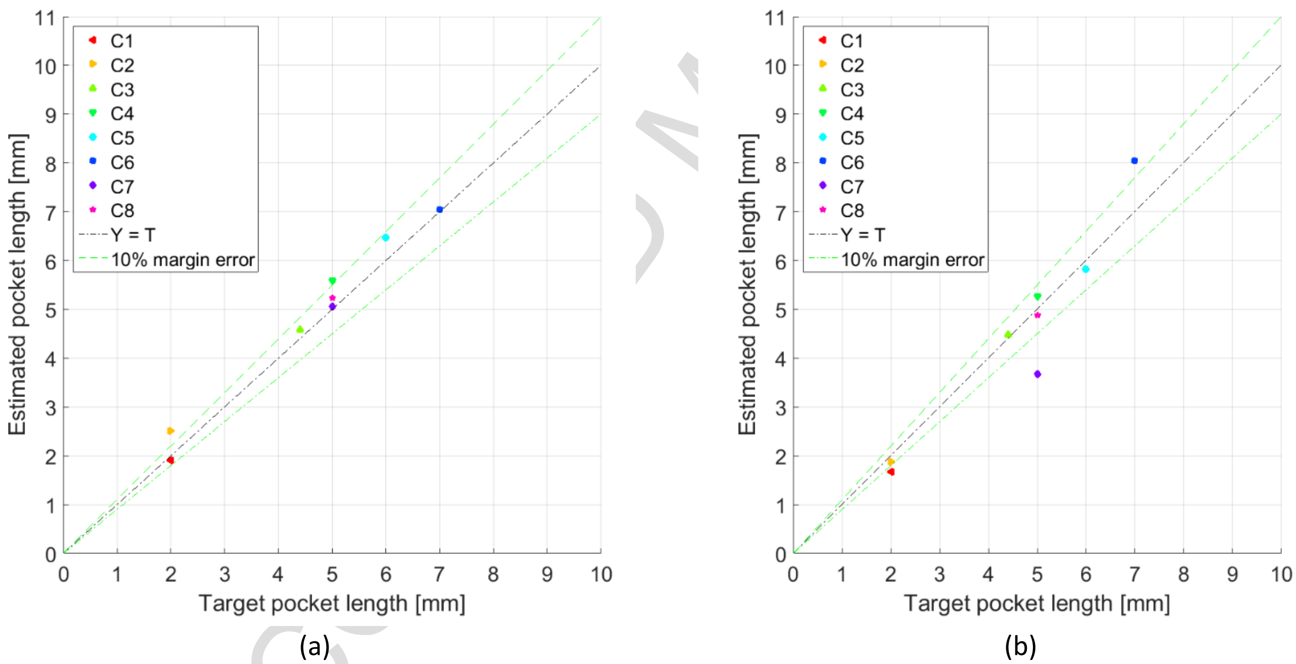

Figure 14 The network predictions of the crack pocket length based on (a) simulation data and (b) experimental ACFM measurements.

Figure 14 shows the result of pocket length predictions based on the inputs provided by simulation and experiments. The results show a validation error of within 10% for most of the clusters in both cases; however, in the case of the experimental data, the prediction errors for C6 & C7 are slightly higher than the rest; this disagreement, however, may be accounted for by the experimental procedure, e.g. change of probe direction or lift-off during the measurements as the measurements were manually taken, and inherent variations and can be improved by using an automated system to perform the measurements more consistently, e.g. 2D raster scans by a robotic arm.

7. Conclusions

The results of the case study presented in this paper show an effective machine learning approach for sizing of clustered cracks. The machine learning approach enables the sizing of clustered cracks using the ACFM technique, whose response to these groups of cracks has been shown to be complex due to the interactions caused by the close proximity of cracks. The previously established methods and look up tables for isolated cracks are invalid in the multiple crack case because they would significantly overestimate the crack size for clustered cracks.

The technique introduced in this paper involves application of a MLP network which is trained using extensive validated modelling data of ACFM responses to clustered cracks, where the complex interaction of different parameters of a crack cluster: surface length, number of cracks, inter-crack spacing and surface length uniformity within a crack cluster, have been taken into account resulting in improved prediction accuracy of crack pocket length of the largest crack in a cluster (i.e. within 10% error) compared to the previously established methods. The method presented in this paper requires a priori information about different parameters of a crack cluster (i.e. S, N, I, M). However, it has potential to be extended to allow prediction of all relevant multiple crack parameters directly from the measurements.

It has been demonstrated for a railway application and has the potential to be incorporated into the software of an ACFM-based inspection system deployed on the railway to increase the reliability of the inspection process. It has the potential to aid the automation of sizing of RCF cracks based on the data obtained from a low speed inspection regime. To implement this technique in a full ACFM inspection system would require further research and potential design improvements of the network to deal with more complex RCF crack clusters on in-service rails which sometimes exhibit significant non-uniformity of the crack parameters within a cluster. The method presented in this paper has the advantage of being a more robust approach compared to using a multi-dimensional lookup table because it requires a smaller database which can be easily adjusted to contain cracks of appropriate dimensions to suit different applications outside the railway domain where clustered cracks appear in metals.

Acknowledgment

Funding to support this research was provided through a knowledge transfer secondment grant (UOBKTS006) with funding from EPSRC and TSC Inspections Ltd.

References

[1] B. A. Auld and J. C. Moulder, "Review of advances in quantitative eddy current nondestructive evaluation," *Journal of Nondestructive Evaluation,* vol. 18, pp. 3-36, 1999.

[2] A. Sophian, G. Y. Tian, and J. Rudlin, "Electromagnetic and eddy current NDT: a review," *Insight - Non-Destructive Testing and Condition Monitoring,* vol. 43, 2001.

[3] C. V. Dodd and W. E. Deeds, "Analytical solutions to the eddy current proble-coil problems," *Journal of Applied Physics,* vol. 39, pp. 2829-2838, 1968.

[4] W. D. Dover, R. Collins, and D. H. Michael, "Review of developments in ACPD and ACFM," *The British Journal of NDT,* vol. 33, pp. 121-127, 1991.

[5] N. Harfield and J. R. Bowler, "Theory of thin-skin eddy-current interaction with surface cracks," *Journal of Applied Physics,* vol. 82, pp. 4590-4603, 1997.

[6] A. Tamburrino, "A communications theory approach for electromagnetic inverse problems," *IEEE Transactions on Magnetics,* vol. 36, pp. 1136-1139, 2000.

[7] W. Lord and R. Palanisamy, "Development of Theoretical Models for Nondestructive Testing Eddy-Current Phenomena," in *Eddy-Current Characterization of Materials and Structures, STP27575S*, G. Birnbaum and G. Free, Eds., ed West Conshohocken, PA: ASTM International, 1981, pp. 5-21.

[8] J. R. Bowler, S. J. Norton, and D. J. Harrison, "Eddy-current interaction with an ideal crack. II. The inverse problem," *Journal of Applied Physics,* vol. 75, pp. 8138-8144, 1994.

[9] J. R. Bowler, "Pulsed eddy-current interaction with subsurface cracks," in *Review of Progress in Quantitative Nondestructive Evaluation*. vol. 18, T. D.O. and C. D.E., Eds., ed Boston, MA: Springer, 1999.

[10] L. Udpa and S. S. Udpa, "Solution of inverse problems in eddy-current non-destructive evaluation," *Journal of Nondestructive Evaluation,* vol. 7, 1988.

[11] J. R. Bowler, "Review of eddy current inversion with application to nondestructive evaluation," *International Journal of Applied Electromagnetics and Mechanics,* vol. 8, pp. 3-16, 1997.

[12] G. Rubinacci, A. Tamburrino, and S. Ventre, "Fast numerical techniques for electromagnetic nondestructive evaluation," *Nondestructive Testing and Evaluation,* vol. 24, 2009.

[13] A. Bernieri, L. Ferrigno, M. Laracca, and M. Molinara, "Crack Shape Reconstruction in Eddy Current Testing Using Machine Learning Systems for Regression," *IEEE Transactions on Instrumentation and Measurement,* vol. 57, pp. 1958-1968, 2008.

[14] L. S. Rosado, F. M. Janeiro, P. M. Ramos, and M. Piedade, "Defect Characterization With Eddy Current Testing Using Nonlinear-Regression Feature Extraction and Artificial Neural Networks," *IEEE Transactions on Instrumentation and Measurement,* vol. 62, pp. 1207-1214.

[15] R. Douvenot, M. Lambert, and D. Lesselier, "Adaptive metamodels for crack characterization in eddy-current testing," *IEEE Transactions on Magnetics,* vol. 47, pp. 746-755, 2011.

[16] M. P. Papaelias and M. Lugg, "Detection and evaluation of rail surface defects using alternating current field measurement techniques," *Proceedings of the Institution of Mechanical Engineers, Part F: Journal of Rail and Rapid Transit,* vol. 226, pp. 530-541, 2012.

[17] D. Hesse and P. Crawley, "Defect detection in rails using ultrasonic surface waves," *Insight - Non-Destructive Testing and Condition Monitoring,* vol. 49, pp. 318-326, 2007.

[18] "Train Derailment at Hatfield: A Final Report by the Independent Investigation Board," Office of Rail Regulation London2006.

[19] R. A. Smith, "The wheel-rail interface – some recent accidents," *Fatigue and fracture of engineering materials and structures,* vol. 26, pp. 901-907, 2003.

[20] G. L. Nicholson, H. Rowshandel, X. J. Hao, and C. L. Davis, "Measurement and modelling of ACFM response to multiple RCF cracks in rail and wheels," *Ironmaking & Steelmaking,* vol. 40, pp. 87-91, 2013.

[21] J. Wilson, G. Tian, I. Mukriz, and D. Almond, "PEC thermography for imaging multiple cracks from rolling contact fatigue," *NDT & E International,* vol. 44, pp. 505-512, 10// 2011.

[22] M. Howitt, "Bombardier brings ACFM into the rail industry," *Insight,* vol. 44, pp. 379-382, 2002.

[23] D. Topp and M. Smith, "Application of the ACFM inspection method to rail and rail vehicles," *Insight - Non-Destructive Testing and Condition Monitoring,* vol. 47, pp. 354-357, 2005.

[24] G. L. Nicholson and C. L. Davis, "Modelling of the response of an ACFM sensor to rail and rail wheel RCF cracks," *NDT & E International,* vol. 46, pp. 107-114, 2012.

[25] J. Shen, "Responses of alternating current field measurement (ACFM) to rolling contact fatigue (RCF) cracks in railway rails," PhD, University of Warwick, 2017.

[26] M. P. Papaelias, C. Roberts, and C. L. Davis, "A review on non-destructive evaluation of rails: state-of-the-art and future development," *Proceedings of the Institution of Mechanical Engineers, Part F: Journal of Rail and Rapid Transit,* vol. 222, pp. 367-384, 2008.

[27] D. F. Cannon, K. O. Edel, S. L. Grassie, and K. Sawley, "Rail defects: an overview," *Fatigue & Fracture of Engineering Materials & Structures,* vol. 26, pp. 865-886, 2003.

[28] R. S. Edwards, S. Dixon, and X. Jian, "Characterisation of defects in the railhead using ultrasonic surface waves," *NDT & E International,* vol. 39, pp. 468-475, 2006.

[29] Y. Li, G. Y. Tian, and S. Ward, "Numerical simulation on magnetic flux leakage evaluation at high speed," *NDT & E International,* vol. 39, pp. 367-373, 2006.

[30] Y. Li, J. Wilson, and G. Y. Tian, "Experiment and simulation study of 3D magnetic field sensing for magnetic flux leakage defect characterisation," *NDT & E International,* vol. 40, pp. 179-184, 2007.

[31] A. Raine and M. Lugg, "A review of the alternating current field measurement inspection technique," *Sensor Review,* vol. 19, pp. 207-213, 1999.

[32] R. Collins, "The development of the ACPD and ACFM techniques at UCL," *Nondestructive Testing of Materials,* vol. 8, pp. 65-74, 1995.

[33] D. Mirshekar-Syahkal, "Review of High Sensitivity AC Field Measurement — Recent Advances and Future Work," in *Review of Progress in Quantitative Nondestructive Evaluation: Volume 17A*, D. O. Thompson and D. E. Chimenti, Eds., ed Boston, MA: Springer US, 1998, pp. 235-242.

[34] E. Resendiz, J. M. Hart, and N. Ahuja, "Automated visual inspection of railroad tracks," *Intelligent Transportation Systems, IEEE Transactions on,* vol. 14, pp. 751-760, 2013.

[35] M. Molodova, Z. Li, A. Nunez, and R. Dollevoet, "Automatic detection of squats in railway infrastructure," *Intelligent Transportation Systems, IEEE Transactions on,* vol. 15, pp. 1980-1990, 2014.

[36] M. Singh, S. Singh, J. Jaiswal, and J. Hempshall, "Autonomous Rail Track Inspection using Vision Based System," in *Computational Intelligence for Homeland Security and Personal Safety, Proceedings of the 2006 IEEE International Conference on*, 2006, pp. 56-59.

[37] O. Zahran and W. Al-Nuaimy, "Automatic segmentation of time-of-flight diffraction images using time-frequency techniques application to rail-track defect detection," *Insight - Non-Destructive Testing and Condition Monitoring,* vol. 46, pp. 338-343, 2004.

[38] H.-M. Thomas, T. Heckel, and G. Hanspach, "Advantage of a combined ultrasonic and eddy current examination for railway inspection trains," *Insight - Non-Destructive Testing and Condition Monitoring,* vol. 49, pp. 341-344, 2007.

[39] T. Szugs, A. Krüger, G. Jansen, B. Beltman, S. Gao, H. Mühmel*, et al.*, "Combination of Ultrasonic and Eddy Current Testing with Imaging for Characterization of Rolling Contact Fatigue," in *19th World Conference on Non-Destructive Testing* Munich, Germany, 2016.

[40] S. Yella, M. S. Dougherty, and N. K. Gupta, "Artificial intelligence techniques for the automatic interpretation of data from non-destructive testing," *Insight - Non-Destructive Testing and Condition Monitoring,* vol. 48, pp. 10-20, 2006.

[41] J.-H. Chou and R. Clark, "Application of neural networks to the inspection of railroad rail," in *Review of progress in quantitative nondestructive evaluation*, D. O. Thompson and D. Chimenti, Eds., ed New York: Plenum Press, 1999, pp. 2121-2128.

[42] C. Alippi, E. Casagrande, F. Scotti, and V. Piuri, "Composite real-time image processing for railways track profile measurement," *IEEE Transactions on Instrumentation and Measurement,* vol. 49, pp. 559-564, 2000.

[43] F. Marino, A. Distante, P. L. Mazzeo, and E. Stella, "A real-time visual inspection system for railway maintenance: Automatic hexagonal-headed bolts detection," *IEEE Transactions on Systems, Man and Cybernetics Part C: Applications and Reviews,* vol. 37, pp. 418-428, 2007.

[44] X. Gibert, V. M. Patel, and R. Chellappa, "Deep Multitask Learning for Railway Track Inspection," *IEEE Transactions on Intelligent Transportation Systems,* vol. 18, pp. 153-164, 2017.

[45] S. Yella, M. Dougherty, and N. K. Gupta, "Condition monitoring of wooden railway sleepers," *Transportation Research Part C: Emerging Technologies,* vol. 17, pp. 28-55, 2009.

[46] J. Yang, "Defect recognition algorithm in online ultrasonic inspection for railway freight car wheel," *China Railway Science,* vol. 37, pp. 102-107, 2016.

[47] J. Shuxiang and S. B. Wong, "Development of an automated ultrasonic testing system," in *Third International Conference on Experimental Mechanics and Third Conference of the Asian Committee on Experimental Mechanics*, Singapore, 2005, pp. 480-486.

[48] Y. Gao, G. Y. Tian, P. Wang, H. Wang, B. Gao, W. L. Woo*, et al.*, "Electromagnetic pulsed thermography for natural cracks inspection," *Scientific Reports,* vol. 7, p. 42073, 02/07/online 2017.

[49] A. M. Lewis, D. H. Michael, M. C. Lugg, and R. J. Collins, "Thin-skin electromagnetic fields around surface-breaking cracks in metals," *Journal of Applied Physics,* vol. 64, pp. 3777-3784, 1988.

[50] G. L. Nicholson, A. G. Kostryzhev, X. J. Hao, and C. L. Davis, "Modelling and experimental measurements of idealised and light-moderate RCF cracks in rails using an ACFM sensor," *NDT & E International,* vol. 44, pp. 427-437, 2011.

[51] G. L. Nicholson, A. G. Kostryzhev, H. Rowshandel, M. P. Papaelias, C. L. Davis, and C. Roberts, "Sizing and tomography of rolling contact fatigue cracks in rails using NDT technology - potential for high speed application," in *Proceedings of the 9th World Conference on Railway Research*, Lille, France, 2011.

[52] J. Shen, L. Zhou, H. Rowshandel, G. Nicholson, and C. Davis, "Determining the propagation angle for non-vertical surface-breaking cracks and its effect on crack sizing using an ACFM sensor," *Measurement Science and Technology,* vol. 26, p. 115604, 2015.

[53] F. J. Franklin, J. E. Garnham, D. I. Fletcher, C. L. Davis, and A. Kapoor, "Modelling rail steel microstructure and its effect on crack initiation," *Wear,* vol. 265, pp. 1332-1341, 2008.

[54] J. E. Garnham, D. I. Fletcher, C. L. Davis, and F. J. Franklin, "Visualization and modelling to understand rail rolling contact fatigue cracks in three dimensions," *Proceedings of the Institution of Mechanical Engineers, Part F: Journal of Rail and Rapid Transit,* vol. 225, pp. 165-178, 2011.

[55] Railtrack, "Permanent Way Special Instruction No. 4, Issue 2," ed, 2002.

[56] M. Lugg, "ACFM Inspection Procedure for AMIGO and ASSIST Family Software," TSC Inspection Systems2008.

[57] M. Ravan, S. H. H. Sadeghi, and R. Moini, "Neural network approach for determination of fatigue crack depth profile in a metal, using alternating current field measurement data," *Science, Measurement & Technology, IET,* vol. 2, pp. 32-38, 2008.

[58] M. Ravan, S. H. H. Sadeghi, and R. Moini, "Using a wavelet network for reconstruction of fatigue crack depth profile from AC field measurement signals," *NDT & E International,* vol. 40, pp. 537-544, 2007.

[59] F. Marino, A. Distante, M. Nitti, and E. Stella, "A real-time visual inspection system for railway maintenance: Automatic rail detection and tracking," *Politecnico di Bari, Italy, Intern. Rep. DEE,* 2005.

[60] L. Qingyong and R. Shengwei, "A Real-Time Visual Inspection System for Discrete Surface Defects of Rail Heads," *Instrumentation and Measurement, IEEE Transactions on,* vol. 61, pp. 2189-2199, 2012.

[61] G. D'Angelo, M. Laracca, S. Rampone, and G. Betta, "Fast Eddy Current Testing Defect Classification Using Lissajous Figures," *IEEE Transactions on Instrumentation and Measurement,* 2018.